IJPAS | INTERNATIONAL JOURNAL PURE AND APPLIED SCIENCES
ISSN: 2149-0910

Vol. 11(1); 1-16 (2025)
DOI:10.29132/ijpas.1592979

Research Article

Investigation of Thermomechanical Buckling Characteristics of Auxetic Core Layered Smart Sandwich Plates

Mustafa Buğday [1*]

[1]Department of Mechanical Engineering, Karabuk University, Karabuk, Turkey;
mustafabugday@karabuk.edu.tr
*Corresponding author

Received: 28.11.2024

Accepted: 07.02.2025

Abstract: This study analytically investigated the thermo-mechanical buckling behavior of smart sandwich plates with auxetic core layer based on the theory of high-order shear deformation. The outer layers of the plate were modeled as $BaTiO_3$ and $CoFe_2O_4$, and the core layer was modeled as nickel material with auxetic cell structure. The equations of motion derived using Hamilton's Principle were solved by Navier method, and the effects of auxetic core properties and electric and magnetic fields were evaluated. Although the analytical model was based on the literature, new equations were developed for the interaction of auxetic core and smart materials. The findings showed that auxetic parameters and external fields have significant effects on the buckling temperature and critical loads. This study provides a theoretical basis for the thermo-mechanical buckling analysis of auxetic core sandwich plates.

Keywords: auxetic structure; smart sandwich plate; magneto strictive material; electro elastic material; thermal buckling

Araştırma Makalesi

Auxetic Çekirdek Katmanlı Akıllı Sandviç Plakaların Termomekanik Burkulma Karakteristiklerinin İncelenmesi

Özet: Bu çalışma, yüksek dereceli kayma deformasyonu teorisini temel alarak, auxetic çekirdek katmanlı akıllı sandviç plakaların termo-mekanik burkulma davranışını analitik olarak incelemiştir. Plakanın dış katmanları $BaTiO_3$ ve $CoFe_2O_4$, çekirdek katmanı ise auxetic hücre yapısına sahip nikel malzeme ile modellenmiştir. Hamilton İlkesi kullanılarak türetilen hareket denklemleri, Navier yöntemiyle çözülmüş, auxetic çekirdek özellikleri ile elektrik ve manyetik alanların etkileri değerlendirilmiştir. Analitik model literatüre dayanmakla birlikte, auxetic çekirdek ve akıllı malzemelerin etkileşimine yönelik yeni denklemler geliştirilmiştir. Bulgular, auxetic parametreler ve harici alanların, burkulma sıcaklığı ve kritik yükler üzerinde önemli etkileri olduğunu göstermiştir. Bu çalışma, auxetic çekirdekli sandviç plakaların termo-mekanik burkulma analizi için teorik bir temel sunmaktadır.

Anahtar Kelimeler: auxetic yapı; akıllı sandviç plaka; manyetostriktif malzeme; elektro elastik malzeme; termal burkulma

1. Introduction

Magneto-electro-elastic (MEE) materials represent a distinct category of smart materials that display piezoelectric and piezomagnetic characteristics in a stratified arrangement [1]. These materials, referred to as multiferroics, have garnered considerable interest due to their capacity to efficiently couple distinct phases, rendering them advantageous in multiple industries [2]. The magnetoelectric coupling effects in MEE materials have resulted in their extensive application in engineering fields, including sensors, actuators, robotics, structural health monitoring, vibration control, and medical instruments [3].

Researchers have investigated the fabrication of multiphase magneto-electro-elastic (MMEE) materials by adjusting the volume fractions of various constituents such as BaTiO3 and CoFe2O4 [4]. Research on magneto-electro-elastic nanoplates has demonstrated that surface effects significantly influence the propagation of anti-plane shear waves in these materials [5]. Furthermore, polymer-based magneto-electro-elastic composites have arisen as promising materials, exhibiting macro-scale magneto-electric coupling through homogenization techniques [6].

Piezo-magnetic plates have garnered attention in numerous research studies centered on intelligent composite materials. A micromechanical model has been created for the examination of smart composite piezo-magneto-thermoelastic thin plates with rapidly fluctuating thickness [7]. These studies encompass thermoelastic damping, orthotropic materials, and finite element methods to analyze the behavior of complex structures [8]. Furthermore, investigations have been undertaken on sandwich nanoplates incorporating piezo-magnetic face-sheets, utilizing theories such as sinusoidal shear deformation plate theory to formulate equations of motion for these structures [9]. Javani et al. [10] examine the temperature-dependent functionally graded material circular plate with piezoelectric sensor/actuator layers in relation to the active control of thermally induced vibrations.

Smart plates, especially those utilizing advanced materials and technologies, provide numerous applications and advantages. These plates can be fabricated through various techniques, including the incorporation of conductive materials into textile structures [11], the application of piezoelectric materials for shape modulation [12], and the use of shape memory polymers for bidirectional shape memory functionality [13]. Moreover, the optimization of piezoelectric sensors and actuators can be achieved for vibration control [14], while laminated structures can be modeled to enhance dynamic stability [15].

Thermal buckling is a significant phenomenon that arises in structures exposed to thermal loads and constraints that restrict their movement [16]. Disregarding thermal stress, which may constitute up to 40% of mechanical stress, poses considerable safety hazards, particularly in aerospace structures [17]. Studies indicate that thermal buckling frequently occurs in materials such as titanium alloy plates, attributed to their low critical thermal buckling temperature, resulting in intricate nonlinear responses under thermal-acoustic loadings [18]. Research has emphasized the necessity of performing thermal buckling analysis to ascertain critical buckling temperatures and modal responses under various thermal loads [19].

The thermomechanical behavior of smart plate systems is a significant and contemporary concern, as previously noted. This study examines the modeling of sandwich plates with auxetic core layers and electroelastic and magnetostrictive surface layers. Higher-order plate theory is employed to precisely characterize the behavior of these plates. A thorough framework is examined for the thermomechanical buckling characteristics of the smart sandwich plate. The results of this study can be applied to the advancement of electromechanical smart systems and applications related to vibration and shock damping in high-temperature environments.

2. Mathematical formulation

Figure 1 illustrates a thick rectangular plate constructed from a metal auxetic core and piezo magnetic materials, with dimensions of length a, width b, and thickness t. It is located between two piezo electromagnetic patches, each with a thickness of h_p.

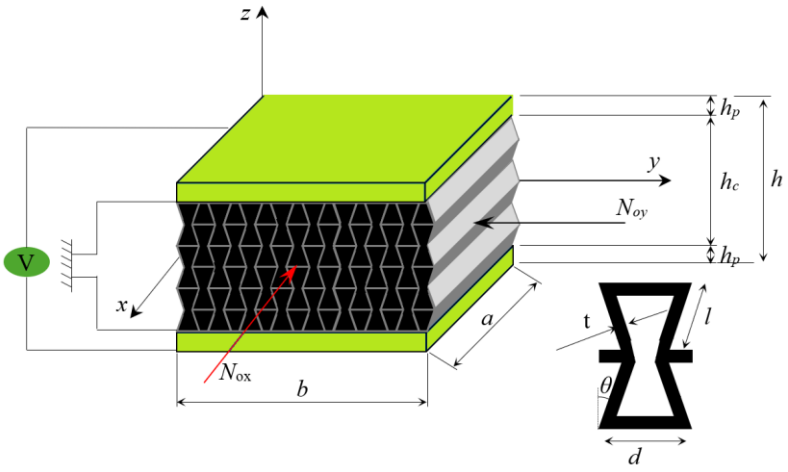

Figure 1. The diagram of the smart sandwich plate and auxetic cell.

The origin is in the central plane, at the midpoint of the plate, and the Cartesian coordinate system is employed for this analysis. The subsequent assumption underpins the present formulation [20]:

1. The three layers of the sandwich plate are seamlessly bonded, eliminating any potential slippage at their interfaces.

2. The characteristics of the upper and lower piezo electromagnetic layers are identical and homogeneous.

In the study, length ratio β_1 and thickness ratio β_3 were calculated as follows:

$$\beta_1 = \frac{l}{d} \tag{1a}$$

$$\beta_3 = \frac{t}{l} \tag{1b}$$

2.1. The types of the temperature increase

Equations for uniform (UTI), nonlinear (NLTI), and linear (LTI) temperature variations are provided for each thickness of the sandwich nanoplate.

Assuming a linear temperature increase (LTI) from the bottom surface T_b to the top surface T_t across the thickness, the temperature of a plane extending along the z-axis can be determined using the following equation [21].

$$T(z) = T_b + (T_t - T_b)\left(\frac{h+2z}{2h}\right) \tag{2}$$

In the case of nonlinear temperature increase (NLTI) across the thickness, the temperatures of the sandwich nanoplate's upper surface T_t and lower surface T_b can be calculated using equation 1 [22].

$$-\frac{d}{dz}\left(\kappa(z)\frac{dT}{dz}\right) = 0, \qquad T\left(\frac{h}{2}\right) = T_t, \quad T\left(-\frac{h}{2}\right) = T_b \tag{3}$$

The temperature of the complete FGM sandwich nanoplate, which experiences a uniform temperature increase from T_0 to T, can be determined using the following equation:

$$\Delta T = T - T_0 \tag{4a}$$

$$T(z) = T_b + \frac{(T_t - T_b)}{\int_{-\frac{h}{2}}^{\frac{h}{2}} \frac{1}{\kappa(z)} d(z)} \int_{-\frac{h}{2}}^{z} \kappa(z)dz \tag{4b}$$

Here, $\kappa(z)$ represents the thermal conductivity coefficient. This study utilizes the nonlinear temperature rise (Eq. 4) for analysis.

2.2. Displacement field

Due to the prominence of shear deformations in the current plate and the necessity for high precision in this system, the displacement field is represented using two SSDT variables, as indicated in [23].

$$u(x,y,z,t) = u_0(x,y,t) - z\frac{\partial w_b(x,y,t)}{\partial x} - f(z)\frac{\partial w_s(x,y,t)}{\partial x}, \tag{5}$$

$$v(x,y,z,t) = v_0(x,y,t) - z\frac{\partial w_b(x,y,t)}{\partial y} - f(z)\frac{\partial w_s(x,y,t)}{\partial y}, \tag{6}$$

$$w(x,y,z,t) = w_b(x,y,t) + w_s(x,y,t) \tag{7}$$

In this context, u_0, v_0, w_b, and ws represent the mid-surface components of displacement, while u, v, and w denote the displacement components of the plate along the x, y, and z axes, respectively. The transverse displacements caused by shearing and bending are denoted by the variables w_s and w_b, respectively. The shape function, $f(z)$, is equivalently expressed as [24]:

$$f(z) = z - \frac{h}{\pi}\sin\left(\frac{\pi z}{h}\right) \tag{8}$$

The components of the strain tensor concerning the displacement field in Equations (1, 2, 3) are as follows:

$$\begin{aligned}
\varepsilon_{xx} &= \frac{\partial u}{\partial x} - z\frac{\partial^2 w_b}{\partial x^2} - f(z)\frac{\partial^2 w_s}{\partial x^2} \\
\varepsilon_{yy} &= \frac{\partial v}{\partial y} - z\frac{\partial^2 w_b}{\partial y^2} - f(z)\frac{\partial^2 w_s}{\partial y^2} \\
\gamma_{xy} &= \frac{\partial v}{\partial x} + \frac{\partial u}{\partial y} - 2z\frac{\partial^2 w_b}{\partial x\,\partial y} - 2f(z)\frac{\partial^2 w_s}{\partial x\,\partial y} \\
\gamma_{yz} &= g(z)\frac{\partial w_s}{\partial y}
\end{aligned} \tag{9}$$

where:

$$g(z) = 1 - f'(z) \tag{10}$$

where the normal strain component is ε_{ii} and the shear strain component is γ_{ij} (ii=xx, yy and ij=xy, yz, xz), respectively.

2.3. Hamilton's principle

The equations of motion are derived utilizing Hamilton's principles. This concept is articulated as follows:

$$\int_{t_1}^{t_2} (\delta U - \delta T - \delta W)\mathrm{d}t = 0 \tag{11}$$

U, T, and W represent external work, kinetic energy, and strain energy, respectively.

2.4. Navier's solution

Analytical solutions exist for equations of motion pertaining to plates with simply supported boundary conditions. The displacements are considered functions that satisfy various geometric boundary conditions according to Navier's solution.

$$\begin{Bmatrix} u_0 \\ v_0 \\ w_b \\ w_s \\ \phi \\ \psi \end{Bmatrix} = \sum_{m=1}^{\infty} \sum_{n=1}^{\infty} \begin{Bmatrix} \bar{u}\cos\left(\frac{m\pi x}{a}\right)\sin\left(\frac{n\pi y}{b}\right) \\ \bar{v}\sin\left(\frac{m\pi x}{a}\right)\cos\left(\frac{n\pi y}{b}\right) \\ \bar{w}_b\sin\left(\frac{m\pi x}{a}\right)\sin\left(\frac{h\pi y}{b}\right) \\ \bar{w}_s\sin\left(\frac{m\pi x}{a}\right)\sin\left(\frac{n\pi y}{b}\right) \\ \bar{\phi}\sin\left(\frac{m\pi x}{a}\right)\sin\left(\frac{n\pi y}{b}\right) \\ \bar{\psi}\sin\left(\frac{m\pi x}{a}\right)\sin\left(\frac{n\pi y}{b}\right) \end{Bmatrix} e^{i\omega t} \quad (12)$$

The maximum values of the displacement components, electric and magnetic potentials, and unknown coefficients are represented by the variables $\bar{u}, \bar{v}, \bar{w}_b, \bar{w}_s, \bar{\phi}$, and $\bar{\psi}$ The natural frequency is denoted as ω.

The following relation is used for the non-dimensional buckling load for the modes m, n:

$$\lambda_{cr}(m,n) = \frac{12(1-v_c^2)N_{cr}a^2}{E_c h^3} \quad (13)$$

For the nondimensional external electric and magnetic potentials the following relations are used.

$$V_m = \frac{V_O}{D_c} \; ; \; D_c = \frac{E_c h^3}{12(1-v_c^2)} \quad (14)$$

$$h_m = \frac{h_O}{h_c} \; ; \; h_c = \frac{E_c h^3}{12(1-h_c^2)} \quad (15)$$

Table 1 presents the magnetic, piezoelectric, electrostatic, and thermal properties of the $CoFe_2O_4$ and $BaTiO_3$ materials utilized. $CoFe_2O_4$ exhibits robust magnetic characteristics and is significant in magneto mechanical interactions. $BaTiO_3$ is an essential material for electromechanical interactions owing to its elevated dielectric constant and piezoelectric responsiveness. These qualities are fundamental parameters for comprehending the response of the core layer in the sandwich structure to external loads. The study meticulously evaluated the effects of the combination of these materials on the system under the influence of magnetic fields, piezoelectric contributions, and thermal loads.

Table 1 The magnetic, piezo, electro and thermal properties of $CoFe_2O_4$ and $BaTiO_3$ [25,26]

		$CoFe_2O_4$	$BaTiO_3$
C_{11}	[GPa]	286	166
C_{22}		286	166
C_{33}		269.5	162
C_{12}		173	77
C_{13}		170.5	78
C_{23}		170.5	78
C_{44}		45.3	43
C_{55}		45.3	43
C_{66}		56.5	44.5
e_{31}	[C/m^2]	0	-4.4
e_{32}		0	-4.4
e_{33}		0	18.6
q_{31}	[N/A.m]	580.3	0
q_{32}		580.3	0
q_{33}		699.7	0
ξ_{11}	[10^{-9}C^2/N.m^2]	0.08	11.2
ξ_{22}		0.08	11.2
ξ_{33}		0.093	12.6
$\zeta_{11} = \zeta_{22} = \zeta_{33}$	[s/m]	0	0
χ_{11}	[10^{-6} N.s^2/C]	-590	5
χ_{22}		-590	5
χ_{33}		157	10
$p_{11} = p_{22}$	[10^{-7}C/m^{2}K]	0	0
p_{33}		0	-11.4
$\lambda_{xx} = \lambda_{yy}$	[10^{-5}Wb/m^{2}K]	0	0
λ_{zz}		-36.2	0
$\alpha_1 = \alpha_2$	[10^{-6}K^{-1}]	10	15.8
ρ	[kg/m^3]	5800	5300

The material characteristics of the auxetic core layer are the fundamental parameters that dictate the mechanical reaction. Table 2 comprises critical engineering data, including modulus of elasticity, density, Poisson's ratio, and thermal expansion coefficient. Auxetic structures have a negative Poisson's ratio, resulting in distinct deformation behavior under mechanical loads compared to conventional materials. This characteristic enhances structural integrity and augments the energy dissipation capability. The study assessed the stability of the auxetic core layer under mechanical and thermal loads, as well as critical buckling loads and deformation characteristics, by considering these material features.

Table 2. Material properties of the Auxetic core layer [27]

Material	Property	P_{-1}	P_0	P_1	P_2	P_3
	ρ (kg/m^3)	0	8900	0	0	0
	E (Pa)	0	223.95x 10^9	-2.794x10^{-4}	3.998x10^{-9}	0
Nickel	υ	0	0.31	0	0	0
	α (1K^{-1})	0	9.9209x10^{-6}	8.705x10^{-4}	0	0
	ψ (W/mK)	0	58.74	-4.614x10^{-4}	6.670x10^{-7}	-1.523x10^{-}

3. Results and Discussion

In the study, a MATLAB based analysis method was applied to evaluate the thermo-mechanical buckling behavior of the sandwich plate, and the obtained data were interpreted through graphs examining the effects of auxetic core parameters, axial compressive force, external electric and magnetic potentials.

3.1. Influence of Auxetic Core Parameters on the Thermal Buckling Behavior of Sandwich Plates

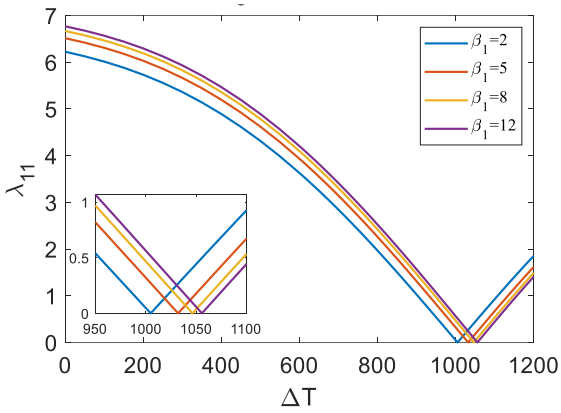

Figure 2. Variation of the dimensionless buckling load λ_{11} of sandwich plate depending on the auxetic length ratio β_1 = 2, 5, 8 and 12; and for auxetic thickness ratio β_3= 0.1; θ=45°; a=1; b=a; h=a/10; h_c = 0.9h; h_p=0.05H; N_x=N_y=0

In Figure 2, the variation of the dimensionless bucking load depending on the Auxetic length ratio and temperature is presented. Here, the analyzes were made for the parameters of the Auxetic core layer, β_3 = 0.1 and θ = 45°. At β_1= 2, while the critical bucking load at ΔT= 0 was λ_{11}= 6.22, at ΔT= 1005 K, bucking occurred by decreasing to λ_{11}= 0. While the critical bucking load at β_1= 5 and ΔT= 0 was λ_{11}= 6.51, bucking occurred by decreasing to λ_{11}= 0 at ΔT= 1032 K. While the critical bucking load at β_1= 8 and ΔT= 0 was λ_{11}= 6.66, bucking occurred by decreasing to λ_{11}= 0 at ΔT= 1046 K. At β_1= 12, while the critical bucking load at ΔT= 0 was λ_{11}= 6.77, bucking occurred by decreasing to λ_{11}= 0 at ΔT= 1055 K.

3.2. Impact of Axial Compression Force on the Thermal Buckling Response of the Sandwich Plate

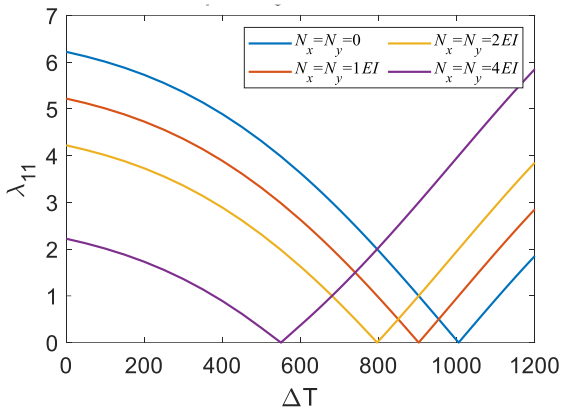

Figure 3. Variation of the dimensionless buckling load λ_{11} of sandwich plate depending on the auxetic length ratio $\beta_1 = 2$; and for auxetic thickness ratio $\beta_3 = 0.1$; θ=45°; a=1; b=a; h=a/10; $h_c = 0.9h$; h_p=0.05h; N_x=N_y=0, 1EI, 2EI, 4EI

Figure 3 shows the variation of dimensionless bucking load depending on axial compression load and temperature. Here, the analyzes were carried out for the parameters of the Auxetic core layer, β_1 = 2, β_3 = 0.1 and θ = 45°. In the case where there is no compression load at $N_x = N_y = 0$, the critical bucking load at ΔT = 0 is λ_{11} = 6.22, while at ΔT = 1003 K, bucking occurs by decreasing to λ_{11} = 0. In the case where the compression load is 1EI at N_x=N_y= 1EI, while the critical bucking load at ΔT= 0 K is λ_{11}= 5.22, at ΔT= 903 K, buckling occurs by decreasing to λ_{11}= 0. In the case where the compression load is 2EI at N_x=N_y= 2EI, while the critical bucking load at ΔT= 0 K is λ_{11}= 4.22, buckling occurs by decreasing to λ_{11}= 0 at ΔT= 796 K. In the case where the compression load is 4EI at N_x=N_y= 4EI, while the critical bucking load at ΔT= 0 K is λ_{11}= 2.22, at ΔT= 550 K, buckling occurs by decreasing to λ_{11}= 0.

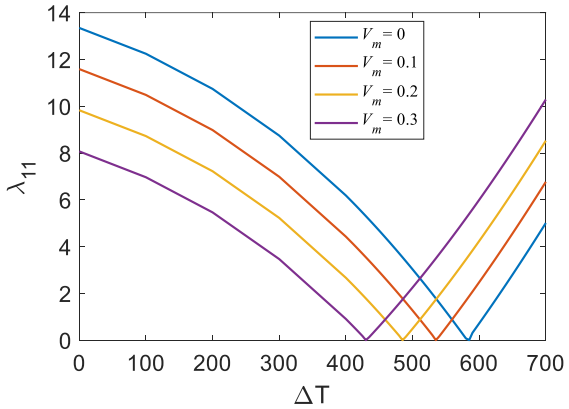

Figure 4. Variation of the dimensionless buckling load λ_{11} of sandwich plate depending on the nondimensional external electric potential V_m= 0, 0.1, 0.2 and 0.3; for θ= 45°, β_1= 2; β_3= 0.1; a=1; b=a; h=a/10; $h_c = 0.2h$; h_p=0.4h; N_x=N_y=0

3.3. Variation in Thermal Buckling Temperature of the Sandwich Plate Under External Electric Potential

As the external electric potential increases, the sandwich plate shows a softening effect due to the electroelastic properties of the surface layers and the buckling temperature decreases.

Figure 4 shows the variation of the dimensionless bucking load depending on external electric potential and temperature. Here, the parameters of the analysis Auxetic core layer was chosen as $\beta_1 = 2, \beta_3 = 0.1$. While the critical bucking load at $V_m = 0$ and $\Delta T = 0$ was $\lambda_{11} = 13.35$, bucking occurred by decreasing to $\lambda 11 = 0$ at $\Delta T = 585$ K. While the critical bucking load at $V_m = 0.1$ and $\Delta T = 0$ was $\lambda_{11} = 11.59$, bucking occurred by decreasing to $\lambda_{11} = 0$ at $\Delta T = 535$ K. While the critical bucking load at $V_m = 0.2$ and $\Delta T = 0$ was $\lambda 11 = 9.83$, bucking occurred by decreasing to $\lambda_{11} = 0$ at $\Delta T = 485$ K. Similarly, at $V_m = 0.3$, while the critical bucking load at $\Delta T = 0$ was $\lambda_{11} = 8.07$, bucking occurred by decreasing to $\lambda_{11} = 0$ at $\Delta T = 430$ K. From $V_m = 0.3$ to $V_m = 0$, the bucking temperature decreased by 1.36 times.

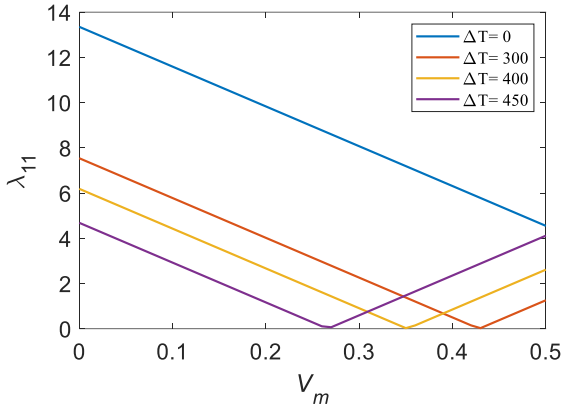

Figure 5. Variation of the dimensionless buckling load λ_{11} of sandwich plate depending on $\Delta T = 0$, 350, 400 and 450; and for the nondimensional external electric potential $V_m = 0$-0.5 $\theta = 45^{\circ}$, $\beta_1 = 2$; $\beta_3 = 0.1$; $a=1$; $b=a$; $h=a/10$; $h_c = 0.2h$; $h_p=0.4h$; $N_x=N_y=0$

Figure 5 shows the variation of the dimensionless bucking load depending on external electric potential and temperature. Here, the parameters of the analysis Auxetic core layer was chosen as $\beta_1 = 2, \beta_3 = 0.1$. At $\Delta T = 0$, critical bucking load at $V_m = 0$ is $\lambda_{11} = 13.35$, where no bucking has occurred. At $\Delta T = 300$, while the critical bucking load was $\lambda_{11} = 7.54$ at $V_m = 0$, bucking occurred by decreasing to $\lambda_{11} = 0$ at $V_m = 0.0277$. While the critical bucking load was $\lambda_{11} = 6.18$ at $\Delta T = 400$, $V_m = 0$, it decreased to $\lambda_{11} = 0$ at $V_m = 0.0273$ and bucking took place. While the critical bucking load was $\lambda_{11} = 4.68$ at $\Delta T = 450$, $V_m = 0$, it decreased to $\lambda_{11} = 0$ at $V_m = 0.067$ and bucking took place.

3.4. Thermal Buckling Behavior of the Sandwich Plate Subjected to External Magnetic Potential

Due to the magneto strictive property of cobalt ferrite in the surface layers of the sandwich plate, a hardening effect occurs on the sandwich plate depending on the magnitude of the external magnetic potential applied and accordingly the buckling temperature decreases.

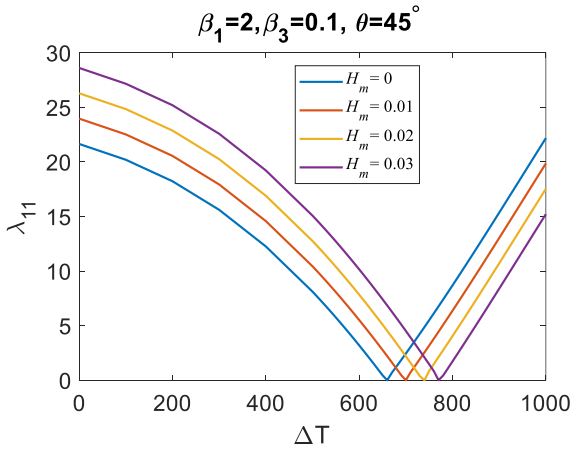

Figure 6. Variation of the dimensionless buckling load λ_{11} of sandwich plate depending on the nondimensional external magnetic potential H_m= 0, 0.01, 0.02 and 0.03; for θ= 45°, β_1= 2; β_3= 0.1; a=1; b=a; h=a/10; h_c = 0.2H; h_p=0.4h; N_x=N_y=0

Figure 6 shows the variation of the dimensionless bucking load depending on external magnetic potential and temperature. Here, the parameters of the analysis Auxetic core layer was chosen as β_1 = 2, β_3 = 0.1. While the critical bucking load at ΔT = 0 and H_m = 0 was λ_{11}= 21.64, at ΔT = 660 K, it decreased to λ_{11}= 0 and buckling took place. While the critical bucking load at ΔT = 0 and H_m = 0.01 was λ_{11}= 23.96, at ΔT = 700 K, it decreased to λ_{11}= 0 and buckling took place. While the critical bucking load was λ_{11}= 26.28 at ΔT = 0 and H_m = 0.02, it decreased to λ_{11}= 0 at ΔT = 740 K and buckling took place. While the critical bucking load was λ_{11}= 28.61 at ΔT = 0 and H_m = 0.03, it decreased to λ_{11}= 0 at ΔT = 770 K and buckling took place. The bucking temperature increased by 1.17 times from H_m = 0.03 to H_m = 0.

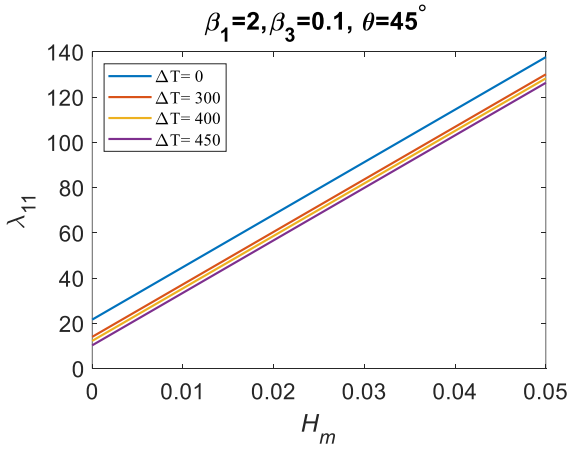

Figure 7. Variation of the dimensionless buckling load λ_{11} of sandwich plate depending on ΔT= 0, 350, 400 and 450; and for the nondimensional external magnetic potential H_m= 0-0.5 θ= 45°, β_1= 2; β_3= 0.1; a=1; b=a; h=a/10; h_c = 0.2h; h_p=0.4h; N_x=N_y=0

Figure 7 shows the variation of the dimensionless bucking load depending on external magnetic potential and temperature. Here, the parameters of the analysis Auxetic core layer was chosen as $\beta_1 = 2$, $\beta_3 = 0.1$. No bucking occurs at $\Delta T = 0$, 300, 400, 450 K. The critical bucking loads occurring at $H_m = 0$ and $\Delta T = 0$, 300, 400, 450 K are $\lambda_{11} = 21.64$, 14.03, 12.25 and 10.28, respectively.

4. Conclusion

This research investigates the modeling and analysis of the thermomechanical buckling characteristics of smart sandwich plates featuring auxetic cores, employing higher-order shear deformation theory. The outer layers of the smart plate comprise electro elastic $BaTiO_3$ (Barium Titanate) and magneto strictive $CoFe_2O_4$ (Cobalt Ferrite) materials. A thorough analysis was performed utilizing the length, thickness, and inclination angle of the auxetic structure to examine the thermomechanical buckling characteristics of the smart sandwich plate. The impact of electric and magnetic potentials on the surface plates of the smart structure regarding backing behavior was examined. The results obtained are summarized as follows:

Comparing the values of the variable length ratio (β_1), constant thickness ratio ($\beta_3 = 0.1$), and constant inclination angle ($\theta = 45°$) reveals that an increase in the length parameter leads to a significant rise in thermal resistance. This phenomenon can be attributed to the fact that a longer auxetic core structure facilitates enhanced energy dissipation and mechanical stability, thereby increasing the temperature at which buckling occurs. The extended length results in a more uniform distribution of thermal stress, delaying the onset of instability in the system.

As axial forces increase from Nx=Ny=0 to Nx=Ny=4EI, the thermal resistance of the axial force exhibits a noticeable increase with respect to the length parameter (β_1=2), constant thickness parameter ($\beta_3 = 0.1$), and fixed inclination angle ($\theta = 45°$). This trend indicates that the applied axial forces reinforce the auxetic core's ability to resist thermal loads by increasing the overall stiffness of the structure. However, as the system reaches a critical state, the accumulation of stress leads to a reduction in the buckling temperature, meaning that under higher axial loads, thermal instability is triggered at lower temperatures. This inverse relationship highlights the trade-off between axial force-induced stiffness enhancement and the loss of thermal stability due to stress accumulation.

When evaluating the external electric potential applied to the auxetic core (β_1=2), with a constant thickness parameter ($\beta_3 = 0.1$) and a fixed inclination angle ($\theta = 45°$), it is evident that an increase in the external electric potential is primarily influenced by the electro elastic effect in the surface layers. The presence of this electric potential generates additional strain within the material, modifying its overall stiffness and stress distribution. This effect, in turn, leads to a decrease in thermal resistance, causing a reduction in the buckling temperature. The results suggest that the electro elastic coupling effect has a destabilizing impact on the structure under thermal loads, reinforcing the importance of accounting for electric field interactions in auxetic core designs.

Similarly, when considering the effect of the external magnetic potential on the auxetic core (β_1=2, $\beta_3 = 0.1$, $\theta = 45°$), it is observed that an increase in the magnetic field intensity contributes to a decrease

in buckling temperature. This reduction is associated with the interaction between the Lorentz forces and the internal mechanical stress distribution within the auxetic core. As the temperature rises, the system becomes increasingly susceptible to premature buckling, particularly under lower magnetic field intensities. This result suggests that although magnetic fields can be used to modulate mechanical stability, excessive exposure to thermal loads under a magnetic field may compromise the overall integrity of the structure.

The findings of this study underscore the complex interplay between geometric parameters, external force fields, and thermal effects on the stability of auxetic core structures. The results demonstrate that while increasing the length parameter enhances thermal resistance and delays buckling, higher axial loads and external electric/magnetic potentials can significantly reduce the critical buckling temperature. These outcomes suggest that optimizing the design of auxetic core structures requires a careful balance between structural dimensions, applied forces, and environmental conditions. Future research could explore adaptive materials with tunable auxetic properties to mitigate the destabilizing effects of thermal and electromagnetic loads. Additionally, experimental validation of the numerical findings would provide deeper insights into the practical implications of the proposed model.

Acknowledgment

The author would like to thank the reviewers and editorial boards of the *International Journal of Pure and Applied Sciences*.

Conflict of Interest

The author asserts that, to the best of his knowledge, he possesses no conflict of interest or shared interest with any institution, organization, or individual that could affect the article's review process.

Author Contribution

This research was independently conducted by Mustafa BUĞDAY. The author executed research design, data collection and analysis, composition, and article editing processes. Throughout this process, ethical guidelines and principles of academic integrity were strictly followed.

Research and Publication Ethics Statement

The author declare that they have complied with the scientific, ethical, and citation principles of the *International Journal of Pure and Applied Sciences* throughout all stages of the study.

References

[1] Mahesh, V., Mahesh, V., Harursampath, D., and Abouelregal, A.E. (2022) Simulation-based assessment of coupled frequency response of magneto-electro-elastic auxetic multifunctional structures subjected to various electromagnetic circuits. *Proceedings of the Institution of Mechanical Engineers, Part L: Journal of Materials: Design and Applications*. 236 (11), 2281–2296.

[2] Moshtagh, E., Eskandari-Ghadi, M., and Pan, E. (2019) Time-harmonic dislocations in a multi-layered transversely isotropic magneto-electro-elastic half-space. *Journal of Intelligent Material Systems and Structures*. 30 (13), 1932–1950.

[3] Park, W.-T. and Han, S.-C. (2018) Buckling analysis of nano-scale magneto-electro-elastic plates using the nonlocal elasticity theory. *Advances in Mechanical Engineering*. 10 (8), 168781401879333.

[4] Mahesh, V. and Kattimani, S. (2019) Finite element simulation of controlled frequency response of skew multiphase magneto-electro-elastic plates. *Journal of Intelligent Material Systems and Structures*. 30 (12), 1757–1771.

[5] Wu, B., Zhang, C., Chen, W., and Zhang, C. (2015) Surface effects on anti-plane shear waves propagating in magneto-electro-elastic nanoplates. *Smart Materials and Structures*. 24 (9), 095017.

[6] Miehe, C. and Vallicotti, D. (2015) Variational Structural and Material Stability Analysis in Finite Electro-Magneto-Mechanics of Active Materials. *PAMM*. 15 (1), 7–10.

[7] Hadjiloizi, D.A., Kalamkarov, A.L., Metti, Ch., and Georgiades, A. V. (2014) Analysis of Smart Piezo-Magneto-Thermo-Elastic Composite and Reinforced Plates: Part I – Model Development. *Curved and Layered Structures*. 1 (1),.

[8] Hadjiloizi, D.A., Kalamkarov, A.L., Metti, Ch., and Georgiades, A. V. (2014) Analysis of Smart Piezo-Magneto-Thermo-Elastic Composite and Reinforced Plates: Part II – Applications. *Curved and Layered Structures*. 1 (1),.

[9] Arefi, M. and Zenkour, A.M. (2016) Employing sinusoidal shear deformation plate theory for transient analysis of three layers sandwich nanoplate integrated with piezo-magnetic face-sheets. *Smart Materials and Structures*. 25 (11), 115040.

[10] Javani, M., Eslami, M.R., and Kiani, Y. (2024) Active control of thermally induced vibrations of temperature-dependent FGM circular plate with piezoelectric sensor/actuator layers. *Aerospace Science and Technology*. 146 108997.

[11] Tseghai, G.B., Malengier, B., Fante, K.A., Nigusse, A.B., and Van Langenhove, L. (2020) Integration of Conductive Materials with Textile Structures, an Overview. *Sensors*. 20 (23), 6910.

[12] Bajoria, K.M. and Patare, S.A. (2021) Shape control of hybrid functionally graded plate through smart application of piezoelectric material using simple plate theory. *SN Applied Sciences*. 3 (2), 209.

[13] Du, H., Yao, Y., Zhou, X., and Zhao, Y. (2023) Two-way shape memory behavior of styrene-based bilayer shape memory polymer plate. *Polymers for Advanced Technologies*. 34 (1), 252–260.

[14] Wang, S.Y., Tai, K., and Quek, S.T. (2006) Topology optimization of piezoelectric sensors/actuators for torsional vibration control of composite plates. *Smart Materials and Structures*. 15 (2), 253–269.

[15] Hoseinzadeh, M. and Rezaeepazhand, J. (2020) Dynamic stability enhancement of laminated composite sandwich plates using smart elastomer layer. *Journal of Sandwich Structures & Materials*. 22 (8), 2796–2817.

[16] Martin, K., Daub, D., Esser, B., Gülhan, A., and Reese, S. (2021) Numerical Modelling of Fluid-Structure Interaction for Thermal Buckling in Hypersonic Flow. in: pp. 341–355.

[17] Deng, W., Wang, B.-W., Lei, K., and Wu, J.-T. (2023) Thermal buckling behavior of metal/composite wall panels. *Journal of Physics: Conference Series*. 2472 (1), 012001.

[18] Zou, X., Guo, D., and Zhang, L. (2015) Dynamic Analysis of the Titanium Alloy Plate under Thermal-acoustic Loadings. *MATEC Web of Conferences*. 35 01005.

[19] Sha, Y.D., Gao, Z.J., Xu, F., and Li, J.Y. (2011) Influence of Thermal Loading on the Dynamic Response of Thin-Walled Structure under Thermo-Acoustic Loading. *Advanced Engineering Forum*. 2–3 876–881.

[20] Ersoy, H., Mercan, K., and Civalek, Ö. (2018) Frequencies of FGM shells and annular plates by the methods of discrete singular convolution and differential quadrature methods. *Composite Structures*. 183 7–20.

[21] Kiani, Y. and Eslami, M.R. (2013) An exact solution for thermal buckling of annular FGM plates on an elastic medium. *Composites Part B: Engineering*. 45 (1), 101–110.

[22] Zhang, D.-G. (2014) Thermal post-buckling and nonlinear vibration analysis of FGM beams based on physical neutral surface and high order shear deformation theory. *Meccanica*. 49 (2), 283–293.

[23] Tornabene, F. and Viola, E. (2009) Free vibration analysis of functionally graded panels and shells of revolution. *Meccanica*. 44 (3), 255–281.

[24] Yuan, W.X. and Dawe, D.J. (2002) Free vibration of sandwich plates with laminated faces. *International Journal for Numerical Methods in Engineering*. 54 (2), 195–217.

[25] Tocci Monaco, G., Fantuzzi, N., Fabbrocino, F., and Luciano, R. (2021) Critical Temperatures for Vibrations and Buckling of Magneto-Electro-Elastic Nonlocal Strain Gradient Plates. *Nanomaterials*. 11 (1), 87.

[26] Esen, I. and Özmen, R. (2024) Free and forced thermomechanical vibration and buckling responses of functionally graded magneto-electro-elastic porous nanoplates. *Mechanics Based Design of Structures and Machines*. 52 (3), 1505–1542.

[27] Esen, I., Abdelrhmaan, A.A., and Eltaher, M.A. (2022) Free vibration and buckling stability of FG nanobeams exposed to magnetic and thermal fields. *Engineering with Computers*. 38 (4), 3463–3482.